AIAA 98-0253

NUMERICAL ANALYSIS OF TRANSIENT COMBUSTION RESPONSES TO ACOUSTIC OSCILLATIONS IN AXISYMMETRIC ROCKET MOTORS

Tae-Seong Roh and Fred E. C. Culick
California Institute of Technology
Pasadena, CA 91125

36th Aerospace Sciences Meeting & Exhibit
January 12–15, 1998 / Reno, NV

Numerical Analysis of Transient Combustion Response to Acoustic Oscillations in Axisymmetric Rocket Motors

T. S. Roh* and F. E. C. Culick†
California Institute of Technology
Pasadena, CA 91125

Abstract

A numerical analysis of unsteady motions in solid rocket motors with a nozzle has been conducted. The formulation treats the complete conservation equations for the gas phase and the one-dimensional equations in the radial direction for the condensed phase. A fully coupled implicit scheme based on a dual time-stepping integration algorithm has been adopted to solve the governing equations and associated boundary conditions. After obtaining a steady state solution, periodic pressure oscillations are imposed at the head end to simulate acoustic oscillations of a traveling-wave motion in the combustion chamber. The amplitude of the pressure oscillation is 1.0 % of the mean pressure and the frequency is 1790 Hz, corresponding to the twice of the fundamental frequency of the chamber. Magnitude and phase of pressure and axial velocity fluctuations are influenced by the upstream reflecting wave from the nozzle wall. Axial velocity near surface region oscillates in phase advance manner with reference to the acoustic pressure. Large vorticity fluctuations are observed in near surface region. The mass-flow-rate at the nozzle exit periodically oscillates with a time delay compared to the imposed pressure oscillations at the head end.

I. Introduction

Combustion instabilities in solid propellant rocket motors have been extensively studied over several decades. Coupled interactions between combustion processes and internal flow dynamics in chamber result in instabilities of motions in combustion chamber. Several modes of interactions between acoustic oscillations and transient combustion have been observed, the most important of which are pressure and velocity coupled responses,[1] denoting the sensitivity of combustion processes to local pressure and velocity fluctuations, respectively. Velocity coupling implies that transient combustion response is strongly influenced by the velocity oscillations parallel to the burning surface, rather than pressure oscillations.[2] Beside pressure and velocity couplings, vorticity is considered as an interaction between acoustic oscillations and transient combustion. Since combustion processes on and near the burning surface control the radial velocity, vorticity fluctuations near the propellant surface are coupled with acoustic pressure and combustion process. Vorticity fluctuations are closely related to the fluctuating radial (or vertical) velocity component upon which system stability is so strongly dependent.[3]

Various approaching methods are required to make progress in understanding mechanisms and behavior of extremely complicated combustion instabilities in solid propellant rocket motors. As one of the methods, the Numerical simulation has provided comprehensive and detailed results applicable to the real rocket motor. In a series of studies on the interactions between acoustic motions and propellant combustion,[4-6] an analysis capable of treating complicated physico-chemical processes involved in unsteady combustion of homogeneous propellants has been developed for two-dimensional Cartesian and axisymmetric combustion chambers. Turbulence closure has been achieved by means of a well-calibrated two-layer model taking into account the effect of propellant surface transport properties. It has been shown that turbulence penetrates into the primary flame zone and consequently increases the propellant burning rate, a phenomenon commonly referred to as erosive burning.[10] The oscillatory flow characteristics are significantly altered by the turbulence due to enhanced momentum and energy transport in the gas phase. A physical insight into the gaseous dynamics and unsteady propellant response has been obtained from analysis of unsteady motions in the combustion chamber. There, however, is a lack of exact simulation of real motor environments because computational domains exclude the nozzle section. Therefore, the purpose of the present work is to conduct a more complete analysis of unsteady behavior in the axisymmetric rocket motor with a nozzle. Emphasis is placed on identifying various distinct features of unsteady flow-fields of the rocket motor in oscillatory environments.

After obtaining a steady state solution shown in

*Post-Doctoral Scholar, AIAA member
†Professor, Fellow AIAA

Ref. 9 for the flow-field of the gas phase, periodic pressure oscillations are imposed at the head end to simulate acoustic oscillations of a traveling-wave motion in the combustion chamber. The amplitude of the pressure oscillation is 1.0 % of the mean pressure and the frequency is 1790 Hz, corresponding to the twice of the fundamental frequency of the chamber. Various aspects of interactions among traveling acoustic oscillations, unsteady reacting flows, and transient propellant combustion are investigated systematically.

II. Theoretical Formulation

Figure 1 shows the situation examined here, an axisymmetric rocket motor. A choked nozzle is attached to the aft end of the combustion chamber. The combustion chamber consists of the gas phase and the condensed phase loaded with a double-base homogeneous propellant grain. The analysis of the gas-phase processes is based on the complete conservation equations of mass, momentum, energy, and species concentration, and takes into account finite-rate chemical kinetics and variations of thermo-physical properties with temperature. Turbulent transport is considered to discuss the effect of turbulent flow disturbances on unsteady heat-release mechanisms. In vector notation, the set of conservation equations for a 2-D axisymmetric combustion chamber including a multi-component chemically reacting system of N species, can be written as

$$\frac{\partial \mathbf{Q}}{\partial t} + \frac{\partial}{\partial x}(\mathbf{E} - \mathbf{E}_v) + \frac{\partial}{\partial y}(\mathbf{F} - \mathbf{F}_v) = \mathbf{S} \qquad (1)$$

where x and y represent the axial and radial coordinates, respectively. The conserved variable vector $\mathbf{Q}$ is defined as

$$\mathbf{Q} = y\left[\rho, \rho u, \rho v, \rho e, \rho k, \rho \epsilon, \rho Y_i\right]^T \qquad (2)$$

where the subscript i stands for the ith species, ranging from 1 to $N-1$, and the superscript T denotes the transpose of the vector. In these equations, ρ, u, v, k, ϵ, and Y_i represent the density, axial and radial velocity components, turbulent kinetic energy, dissipation rate of turbulent kinetic energy, and mass fraction of species i, respectively. Convective flux vectors $\mathbf{E}$ and $\mathbf{F}$ in the axial and radial directions, respectively, take the from

$$\mathbf{E} = y\left[\rho u, \rho u^2 + p, \rho uv, (\rho e + p)u, \rho uk, \rho u\epsilon, \rho uY_i\right]^T \qquad (3)$$

$$\mathbf{F} = y\left[\rho v, \rho uv, \rho v^2 + p, (\rho e + p)v, \rho vk, \rho v\epsilon, \rho vY_i\right]^T \qquad (4)$$

Diffusion-flux vectors $\mathbf{E}_v$ and $\mathbf{F}_v$ are defined below.

$$\mathbf{E}_v = y\left[0, \tau_{xx}, \tau_{xy}, u\tau_{xx} + v\tau_{xy} + q_{e_x}, \tau_{xk}, \tau_{x\epsilon}, q_{i_x}\right]^T \qquad (5)$$

$$\mathbf{F}_v = y\left[0, \tau_{xy}, \tau_{yy}, u\tau_{xy} + v\tau_{yy} + q_{e_y}, \tau_{yk}, \tau_{y\epsilon}, q_{i_y}\right]^T \qquad (6)$$

The τ and q denote normal and shear stresses and species diffusion, respectively. The source vector S includes all source terms associated with the axisymmetric geometry and all remaining terms. The detail description for the complete conservation equations are shown in Ref. 9.

Turbulence closure has been achieved based on the two-layer model of Rodi[11] because of its superior performance over conventional low-Reynolds-number k-ϵ schemes in terms of numerical accuracy and convergence. For unsteady calculations, the empirical constants in the turbulent equations have been corrected based on the study of Fan and Lakshminarayana.[12]

For a multi-component mixture, pressure and temperature can be calculated iteratively from the thermodynamic relation and equation of state. Within the pressure and temperature ranges of practical rocket-motor environments, thermal conductivity and viscosity of each species are basically functions of temperature alone. They can be well approximated by fourth-order polynomials in temperature, with the coefficients of these polynomials supplied by McBride et al.,[13] valid for temperatures ranging from 300 to 6000 K. Thermal conductivity and viscosity are calculated using Wilke's mixing rule.[14]

Condensed-Phase Process

The condensed phase consists of a preheated zone and a superficial degradation layer in which both thermal decomposition of the propellant and reaction of the decomposed species takes place simultaneously. If we ignore the bulk motion, mass diffusion, and axial thermal diffusion, and assume constant thermo-physical properties, the condensed-phase processes are governed by a set of one-dimensional equations in the radial direction. The boundary condition at the condensed-phase far-field is $T = T_i$, where T_i is the initial (conditioned) temperature of the propellant. The surface conditions require that $T = T_s$, where T_i is the burning surface temperature.

Chemical Kinetics Model

Owing to the difficulties in establishing a complete chemical kinetics scheme and limitations of computational resources, a thorough consideration of all physical and chemical processes does not appear feasible. A reduced reaction mechanism is therefore used to describe the combustion wave structure in both the gas and condensed phases. The chemical kinetics used here follow the model established in Ref. 7. This model is a viable alternative which provides well-resolved and reasonably accurate information about major chemical kinetic pathways.

Boundary Conditions

The processes in the gas and condensed phases are matched at the propellant surface by requiring continuity of mass and energy. This procedure ultimately determines the propellant burning rate, temperature, and species concentrations at the surface. Conservation laws are applied to mass and species balances at the gas-solid interface. For unsteady calculations, the energy balance at the interface is also considered. Additionally, the no-slip condition along the axial direction is enforced on the propellant surface and the nozzle wall, where pressure is obtained from the momentum balance. Flow symmetry is assumed to specify the variables along the center line. Boundary conditions at the head end require that the pressure gradient and axial velocity be zero. A second-order extrapolation are adopted at the nozzle exit to obtain boundary variables in supersonic condition.

IV. Numerical Method

A convenient and systematic procedure to convert two-dimensional Cartesian codes into 2-D axisymmetric codes has been proposed.[15] Even though careful calculations of the volume and surface areas of the control volume is considered, a singularity problem is inevitably encountered in certain cases of 2-D axisymmetric calculations. In order to avoid this problem, the governing equations have been modified and solved as if they are two-dimensional Cartesian equations.

$$\frac{\partial \hat{\mathbf{Q}}}{\partial t} + \frac{\partial}{\partial x}\left(\hat{\mathbf{E}} - \hat{\mathbf{E}}_v\right) + \frac{\partial}{\partial y}\left(\hat{\mathbf{F}} - \hat{\mathbf{F}}_v\right) = \mathbf{S}_n \qquad (7)$$

where the superscript ˆ denotes that there is no y term in each vector, and the new source vector can be expressed as

$$\mathbf{S}_n = \hat{\mathbf{S}} - (\hat{\mathbf{F}} - \hat{\mathbf{F}}_v) \qquad (8)$$

This set of governing equations is solved numerically by means of a finite-volume approach. An dual time-stepping integration method[5] proven to be quite efficient and robust for reacting flows at all speeds has been adopted to study the unsteady behavior in the combustion chamber of the solid rocket motor. A fully-coupled implicit formulation is used to enhance numerical stability and efficiency.

III. Calculations

The computational grid system is the same as shown in Ref. 9. The combustion chamber, has a mean pressure of 60 atm, is closed upstream, and measures 5.08 cm in diameter and 0.6 m in length. The computational grid for the combustion chamber consists of 50 × 80 points in the axial and radial directions, respectively, while the condensed-phase grid is composed of 50 × 50 points in the same respective directions. The nozzle contour is delineated by a third-order polynomial in the axial coordinate, with the throat diameter being 2.3 cm. The nozzle has 30 × 80 mesh points of computational grid. The grids of the combustion chamber are clustered near the burning surface in the radial direction to resolve the steep gradients of temperature and species concentrations occurring in the condensed-phase near field. The maximum grid aspect ratio in the combustion chamber is around 10,000. Major ingredients of the propellant are 52% NC and 43% NG, and the thermo-chemical parameters used in the present study are listed in Ref. 7.

The steady-state flow field must be obtained first to provide the initial conditions for analysis of unsteady motions. Calculation results for the flow-field of the gas phase are illustrated in Ref. 9. After obtaining a steady state solution, periodic pressure oscillations are imposed at the head end to simulate acoustic oscillations of a traveling-wave motion in the combustion chamber. The amplitude of the pressure oscillation is 1.0 % of the mean pressure and the frequency is 1790 Hz, corresponding to the twice of the fundamental frequency of the chamber.

V. Results and Discussions

Figure 2 presents time history of pressure oscillations at various axial locations. Amplitudes of Pressure oscillations slightly increases after 2 cycle of oscillations. In case of the axial location X/L = 0.5 (L denotes axial combustion-chamber length), however, pressure oscillations undergo slight change in amplitude and phase. Power of pressure oscillations in Fig. 3 indicates pressure oscillations at X/L=0.5 imply a lower frequency oscillation. The dominating frequency, however, is still the same as the imposed frequency. The reason of the change in pressure oscillations after a few cycles is assumed that the downstream traveling wave be confronted with the upstream propagating wave reflected at the nozzle wall. Magnitude and phase of the reflecting wave seem to be around 20 % and 90 degrees of those of imposed oscillations, respectively. Figure 4 and 5 shows the corresponding contour plot of the traveling wave. The low Mach-number environment basically renders a one-dimensional pressure field, with no discernible variation in the radial direction, which is the same as the result of two-dimensional Cartesian calculations.[7]

The evolutions of the axial velocity fluctuations at four different times within one cycle of oscillations are shown in Figs. 6 and 7. Boundary-layer-type distributions of axial velocity fluctuations are observed but the complex structure near the head-end region shown in a laminar acoustic boundary layer [7] are not clearly found.

Figures 8-11 present time history of axial velocity fluctuations at various radial locations. The radial location, Y/H=1.00 denotes near surface region (primary flame zone), Y/H=0.99 darkzone region (in case of laminar flow), Y/H=0.01 core region, respectively (H represents radius of combustion chamber). Unlike time history of pressure oscillations, as a whole, the magnitude of axial velocity fluctuations in core region decrease at axial locations X/L=0.25 and 0.75 while it increases at axial location X/L=0.5 after a few cycles. With careful examination, the phenomena are also found regardless of radial locations. This implies the downstream traveling waves are influenced by the upstream reflecting waves, same as the case of pressure oscillations. The influenced waves show a slight trend of standing wave properties even though traveling wave property is still dominating in an entire oscillatory environment. The axial velocity fluctuations near surface region in Fig. 8 show a phase advance of 90 degrees with reference to those of core region which follow the isentropic relation with the acoustic pressure. Those at Y/H=0.99 show around 60 degrees of phase advance, also. Therefore, as the radial location moves toward the propellant surface, the phase of the acoustic velocity increases with respect to the acoustic pressure. This phenomenon is also found in Fig. 9 and 10 which show the axial velocity fluctuations at axial locations, X/L=0.5 and 0.75, respectively. Axial velocity fluctuations at the end of the combustion chamber(Fig. 11) hardly exhibit the radial variation of same phase difference as shown in inner axial locations. A slight phase lag in axial velocity fluctuations, on the contrary, is revealed near propellant surface. Besides, magnitudes of the fluctuations at the chamber end are larger than those of inner chamber. Magnitude increase at the chamber end implies the oscillations are affected by reflected waves on the rigid wall, the nozzle wall. This also supports the fact that reflecting waves from the nozzle wall exist in the combustion chamber even though they play a minor role in an oscillatory environment. Figures 12 and 13 show the vertical distributions of amplitudes and phases of axial velocity fluctuations at various axial locations. The amplitude reveals a slight trace of a shear wave near the propellant surface and an isentropic relation with acoustic pressure in core region. Figure 13 clearly shows the phase difference mentioned above.

The contour of vorticity fluctuations is shown in Fig. 14. Large vorticity fluctuations are observed in near surface region opposite to the axial velocity fluctuations because only velocity changes of near surface region play an important role in vorticity fluctuations. In reality, axial velocity change along the radial direction in the core region is almost zero even though it looks much larger than that of near surface region. Fluctuations of vorticity responds to the pressure wave in phase-lag manner. Phase delay of vorticity fluctuations, however, is almost linear from the surface. Time evolutions of vorticity fluctuations at various axial locations are shown in Figs. 15-18. As the axial location moves to the end of the combustion chamber, the extent which has vorticity fluctuations reduces toward the propellant surface.

Figure 19 shows the time average of $< p'v' >$ on the propellant surface. Acoustic admittance is defined as the response of vertical velocity fluctuations to local pressure fluctuations.[16] The real part of acoustic admittance is proportional to the product of pressure and velocity fluctuations within one period of acoustic oscillations $< p'v' >$. Physically, $< p'v' >$ acts like a piston which pumps acoustic energy into the core flow region if the value is positive, and vice versa. Negative value region in Fig. 19 implies that all vertical velocity responses out of phase with acoustic pressure, which predicts the damping effect. Figure 20 reveals $< p'v' >$ in core region at various axial locations. Different from the surface, value of $< p'v' >$ near the head end is only positive.

The contours of temperature fluctuations are shown in Figs. 21 and 22. Temperature changes are mostly observed in flame zones, including large temperature fluctuations near surface region in the vicinity of the axial location X/L= 0.75, where the luminous flame zone merges with the primary flame zone because of the turbulence-enhanced heat transfer. Figures 23-26 show the vertical distributions of temperature fluctuations at various axial locations. At axial location X/L=0.25 (Fig. 23), temperature fluctuations are clearly exhibited in both primary and luminous flame zones. Temperature at axial locations, X/L=0.50 and 0.75 (Figs. 25 and 26) oscillates as if there exists a single-stage flame zone near the propellant surface.

Time evolutions of the heat-release fluctuations at various axial locations are presented in Figs. 27-30. Large fluctuations occur in the secondary flame zone near the head end region, while the downstream region shows a small amplitude of heat release fluctuations, similar to the behavior observed for the temperature fluctuations. Since enhanced mixing processes due to turbulence distribute the chemical reaction over the entire reacting zone (rather than having a strongly exothermic reaction concentrated in the thin secondary flame zone), the amplitudes of temperature and heat-release fluctuation decrease in the downstream region. It is also shown that heat-release fluctuation follows the gradient of the temperature fluctuation.

The effect of heat release on motor stability characteristics can be investigated using Rayleigh's criterion,[17,18] which determines the conditions for driving or suppressing flow oscillations when thermal energy is added (or subtracted) periodically to (or from) the acoustic field.

The Rayleigh's criterion results for various axial locations are presented in Fig. 31. Owing to the reduced heat-release fluctuations, the Rayleigh parameter $< p'q' >$, contains small values in the down stream region. The region which tends to drive the flow oscillations in a rocket motor due to nonsteady heat-release fluctuations agrees with the result shown in Fig. 19.

Figure 32 show time history of surface temperature fluctuations at the various locations. Primary flame behavior is strongly related to the combustion characteristics of the condensed phase. Large surface temperature fluctuations at the end of the combustion chamber are closely related to the mass-flow-rate fluctuations on the propellant surface shown in Fig. 33. The mass-flow-rate at the nozzle exit periodically oscillates with a time delay compared to the imposed pressure oscillations at the head end.

VI. Conclusions

A numerical analysis of unsteady motions in solid rocket motor with a nozzle has been conducted. The formulation considers a 2-D axisymmetric combustion chamber and treats the complete conservation equations, accounting for turbulence closure and finite-rate chemical kinetics in the gas phase and subsurface reactions. The governing equations have been modified and solved as two-dimensional Cartesian equations. A fully-coupled implicit scheme based on a dual time-stepping integration algorithm has been adopted to solve the governing equations and associated boundary conditions.

After obtaining a steady state solution, periodic pressure oscillations are imposed at the head end to simulate acoustic oscillations of a traveling-wave motion in the combustion chamber. The amplitude of the pressure oscillation is 1.0 % of the mean pressure and the frequency is 1790 Hz, corresponding to the twice of the fundamental frequency of the chamber. The low Mach-number environment basically renders a one-dimensional pressure field, with no discernible variation in the radial direction, which is the same as the result of two-dimensional Cartesian calculations. Due to influence of upstream reflecting waves from the nozzle wall, magnitude decreases of pressure oscillations at X/L=0.5 and axial velocity oscillations at X/L=0.25 and 0.75 and magnitude increases of Pressure oscillations at X/L=0.25 and 0.75 and axial velocity oscillations at X/L=0.5 have been detected. The influenced waves have a slight trend of standing wave properties even though traveling wave property is still dominating in an entire oscillatory environment. As the radial location moves toward the propellant surface, the phase of the acoustic velocity increases with respect to the acoustic pressure except for the end of the combustion chamber.

Large vorticity fluctuations are observed in near surface region opposite to the axial velocity fluctuations because only velocity changes in near surface region play an important role in vorticity fluctuations. As the axial location moves to the end of the combustion chamber, the extent which has vorticity fluctuations reduces toward the propellant surface. The time average of $< p'v' >$ on the propellant surface predicts that there are two regions which have driving and damping effect on acoustic oscillations. Temperature changes are mostly observed in flame zones, including large temperature fluctuations near surface region in the vicinity of the axial location X/L= 0.75. According to the result of the Rayleigh parameter $< p'q' >$, the region which have driving effect on the acoustic oscillations agrees with the result of the time average of $< p'v' >$. The mass-flow-rate at the nozzle exit periodically oscillates with a time delay compared to the imposed pressure oscillations at the head end.

References

[1] Culick, F. E. C., "Stability of Longitudinal Oscillations with Pressure and Velocity Coupling in a Solid Propellant Rocket," *Combustion Science and Technology*, Vol.2, No. 4, 1970, pp. 179-201.

[2] Price, E. W., "Velocity Coupling in Oscillatory Combustion of Solid Propellants," *AIAA Journal*, Vol. 17, 1979, pp. 799-800.

[3] Flandro, G. A., "Effect of Vorticity on Rocket Combustion Stability," *Journal of Propulsion and Power*, Vol. 11, No. 4, July 1995.

[4] Culick, F. E. C. and Yang, V., "Prediction of the Stability of Unsteady Motions in Solid Propellant Rocket Motors," *Nonsteady Burning and Combustion Stability of Solid Propellants;* edited by L. De Luca, E. W. Price, and M. Summerfield, Progress in Astronautics and Aeronautics, Vol. 143, 1992, pp. 719-779.

[5] Tseng, I. S. and Yang, V., "Combustion of a Double-Base Homogeneous Propellant in a Rocket Motor," *Combustion and Flame*, Vol. 96, 1994, pp. 325-342.

[6] Roh, T. S. and Yang, V., "A Comprehensive Analysis of Combustion Instabilities of Homogeneous Propellants in A Rocket Motor," *AIAA Paper* 95-2863, 1995 (also submitted to *Journal of Propulsion and Power*).

[7] Roh, T. S., Tseng, I. S., and Yang, V., "Effects of Acoustic Oscillations on Flame Dynamics of Homogeneous Propellants in Rocket Motors," *Journal of Propulsion and Power*, Vol. 11, No. 4, July 1995.

[8] Roh, T. S. and Yang, V., "Numerical Analysis of Combustion Instabilities of Homogeneous Propellants in Axisymmetric Rocket Motors," *AIAA Paper* No. 96-2623, July 1996.

[9] Roh, T. S. and Culick, F.E.C., "Transient Combustion Responses of Homogeneous Propellants to Acoustic Oscillations in Axisymmetric Rocket Motors," *AIAA Paper* No. 97-3325, July 1997.

[10] King, M. K., "Erosive Burning of Solid Propellants," *Journal of Propulsion and Power*, Vol. 9, No. 6, 1993.

[11] Rodi, W., "Experience with Two-Layer Models Combining the $k-\epsilon$ Model with a One-Equation Model near the Wall," *AIAA Paper* No. 91-0216, 1991.

[12] Fan, S. and Lakshminarayana, B., "Low-Reynolds-Number $k-\epsilon$ Model for Unsteady Turbulent Boundary-Layer Flows." *AIAA Journal*, Vol. 31, No. 10, October 1993, pp. 1777-1784.

[13] McBride, B. J. and Gordon, S., *Computer Program for Calculation of Complex Chemical Equilibrium Compositions, Rocket Performance, Incident and Reflected Shocks, and Chapman-Jouguet Detonations*, NASA SP-273, March 1976.

[14] Reid, R. C., Prausnitz, J. M., and Poling, B. E., *The Properties of Gases and Liquids*, 4th Ed., McGraw-Hill Publishing Co., New York, NY, 1987, pp. 577-597.

[15] Yu, S., "Convenient Method to Convert Two-Dimensional CFD Codes into Axisymmetric Ones," *Journal of Propulsion and Power*, Vol. 9, No. 3, 1993, pp. 493-495.

[16] T'ien, J.S., "Theoretical Analysis of Combustion Instability," Fundamentals of Solid-Propellant Combustion, AIAA Progress in Astronautics and Aeronautics, Vol.90, 1984, pp. 791-840.

[17] Rayleigh, J. W. S., *Theory of Sound*, Vol. II., Dover, New York, 1954

[18] Culick, F. E. C., "A Note on Rayleigh's Criterion" *Combustion Science and Technology*, Vol. 56, 1987, pp. 159-166

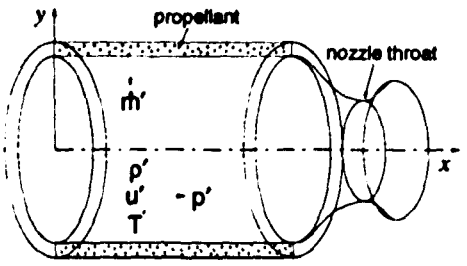

Figure 1: Schematic diagram of a solid rocket motor.

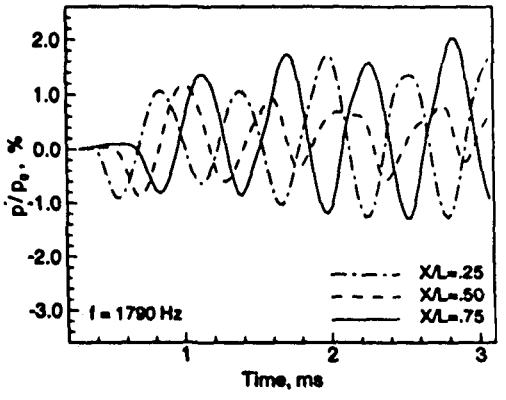

Figure 2: Time history of pressure oscillations at various axial locations.

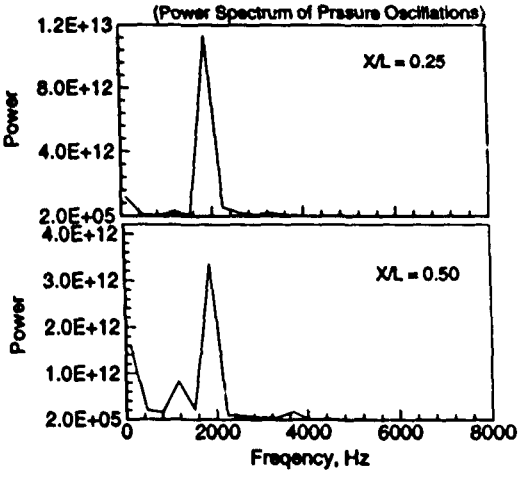

Figure 3: Power spectrum of pressure oscillations at two different axial locations.

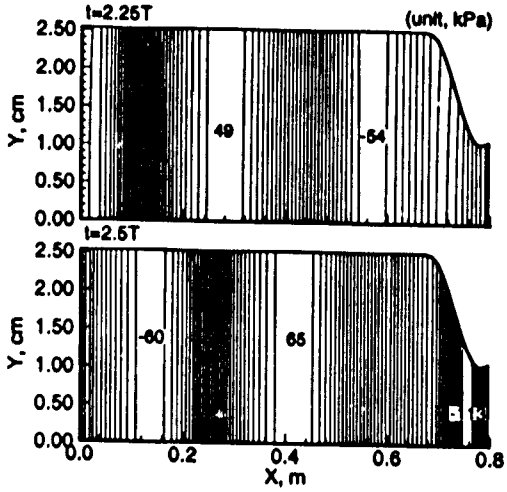

Figure 4: Contour plot of propagation of pressure oscillations on t = 2.25T - 2.50T

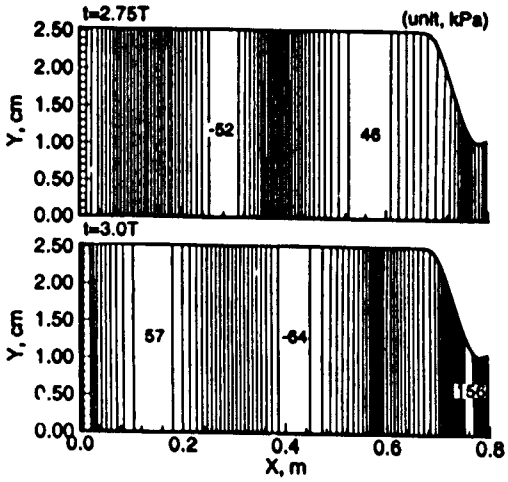

Figure 5: Contour plot of propagation of pressure oscillations on t = 2.75T - 3.0T

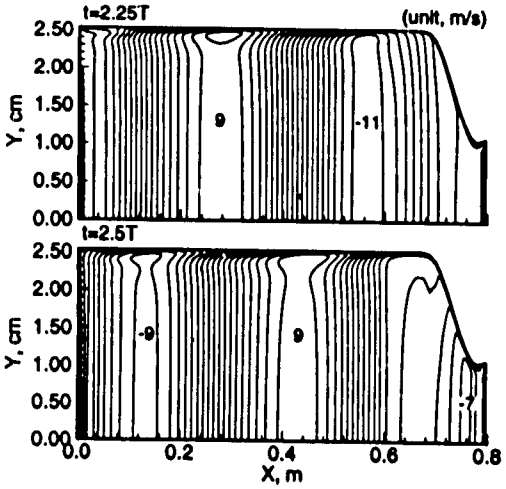

Figure 6: Contour plot of axial velocity fluctuations on t = 2.25T - 2.50T

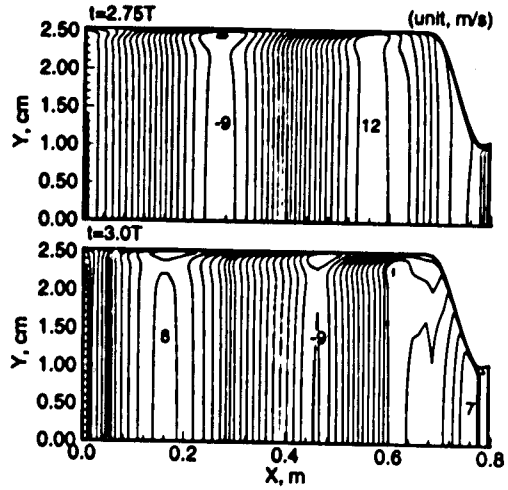

Figure 7: Contour plot of axial velocity fluctuations on t = 2.75T - 3.0T

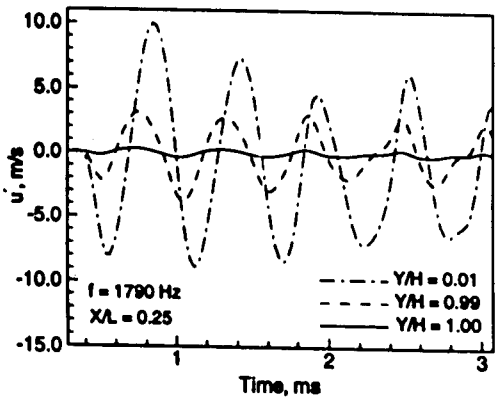

Figure 8: Time evolution of axial velocity fluctuations at axial location, X/L = 0.25

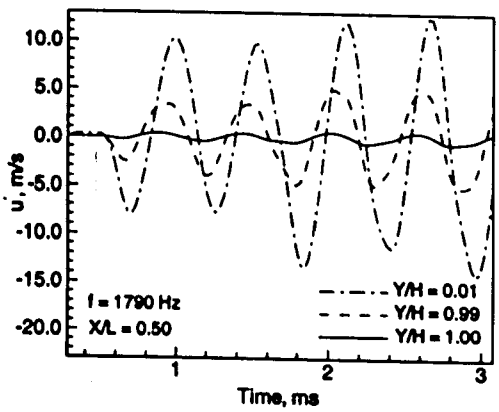

Figure 9: Time evolution of axial velocity fluctuations at axial location, X/L = 0.50

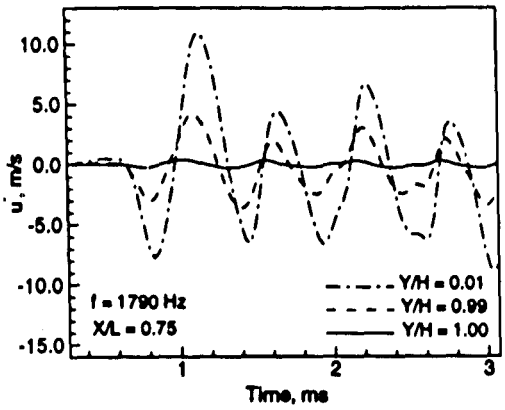

Figure 10: Time evolution of axial velocity fluctuations at axial location, X/L = 0.75

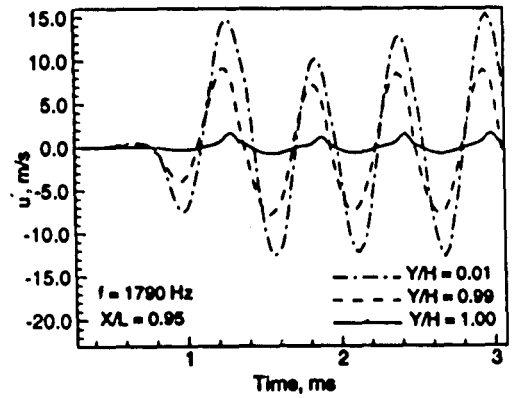

Figure 11: Time evolution of axial velocity fluctuations at axial location, X/L = 0.95

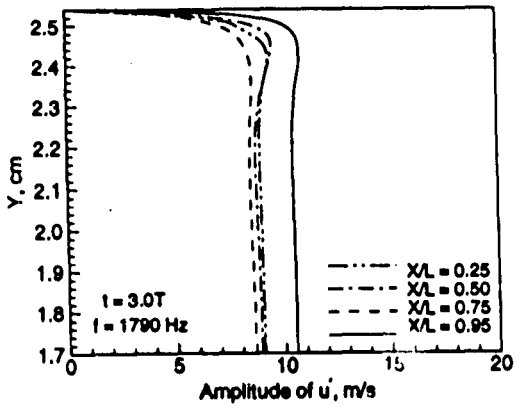

Figure 12: Amplitude of axial velocity fluctuations at various axial locations

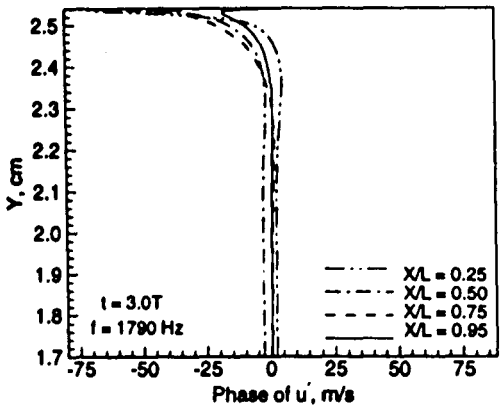

Figure 13: Phase of axial velocity fluctuations at various axial locations

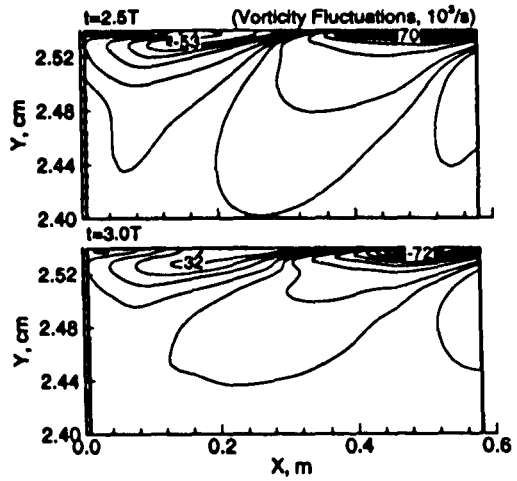

Figure 14: Contour plot of vorticity fluctuations on t = 2.50T - 3.0T

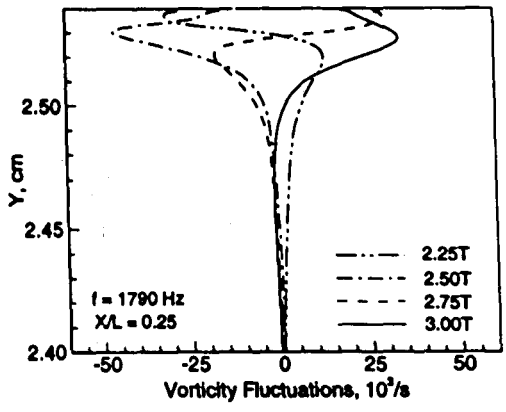

Figure 15: Time evolution of vorticity fluctuations at axial location, X/L = 0.25

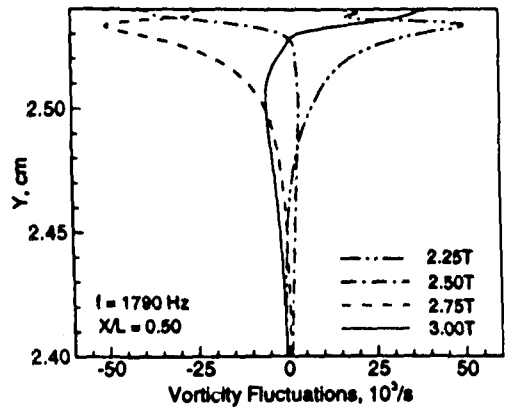

Figure 16: Time evolution of vorticity fluctuations at axial location, X/L = 0.50

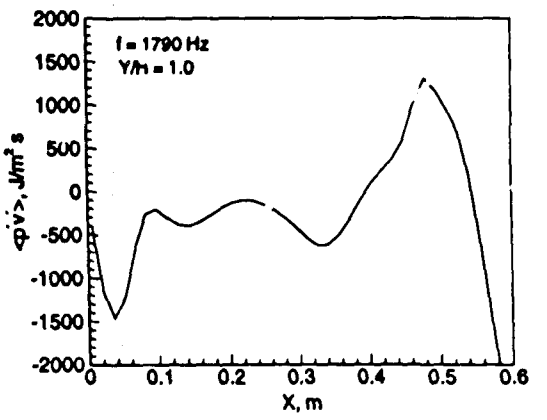

Figure 19: Time average of $< p'v' >$ on propellant surface at t = 5.0T

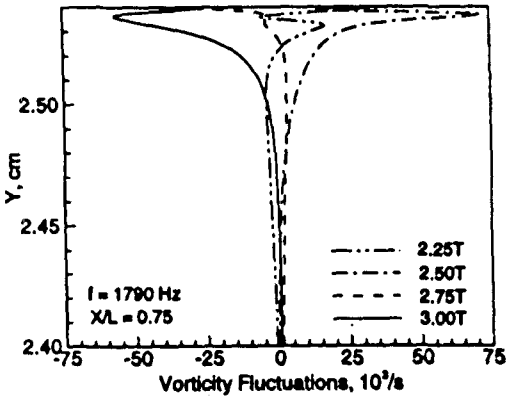

Figure 17: Time evolution of vorticity fluctuations at axial location, X/L = 0.75

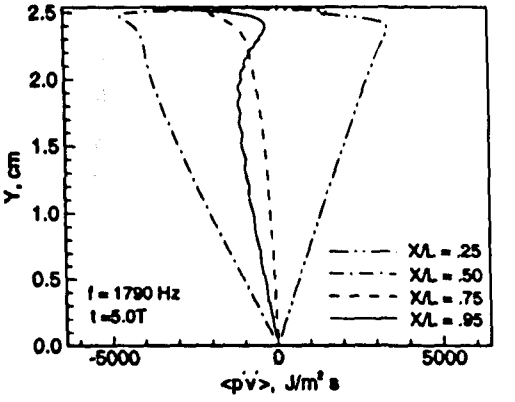

Figure 20: Time average of $< p'v' >$ on propellant surface at various axial locations

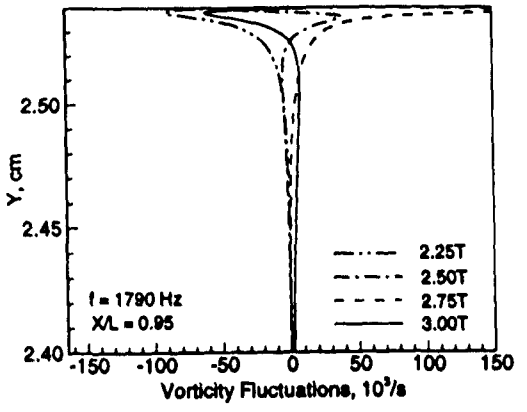

Figure 18: Time evolution of vorticity fluctuations at axial location, X/L = 0.95

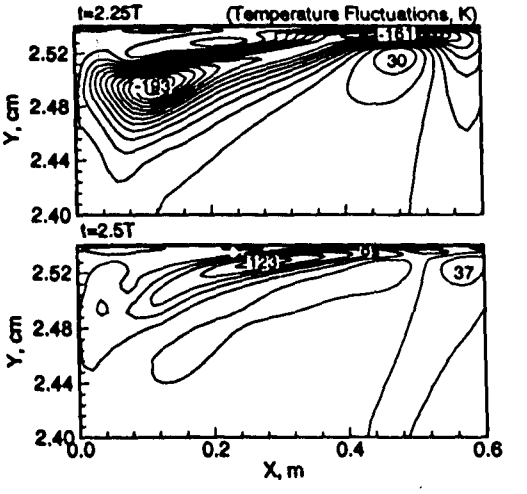

Figure 21: Contour plot of temperature fluctuations on t = 2.25T - 2.50T

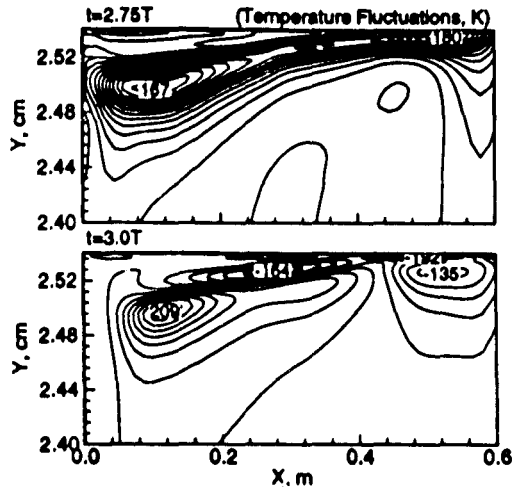

Figure 22: Contour plot of temperature fluctuations on t = 2.75T - 3.0T

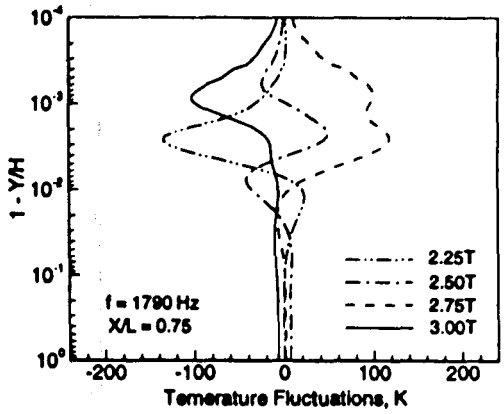

Figure 25: Time evolution of temperature fluctuations at axial location, X/L = 0.75

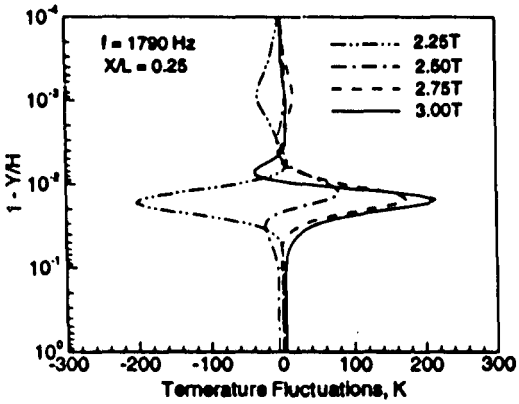

Figure 23: Time evolution of temperature fluctuations at axial location, X/L = 0.25

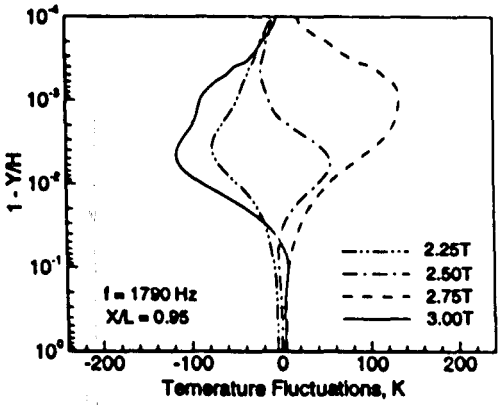

Figure 26: Time evolution of temperature fluctuations at axial location, X/L = 0.95

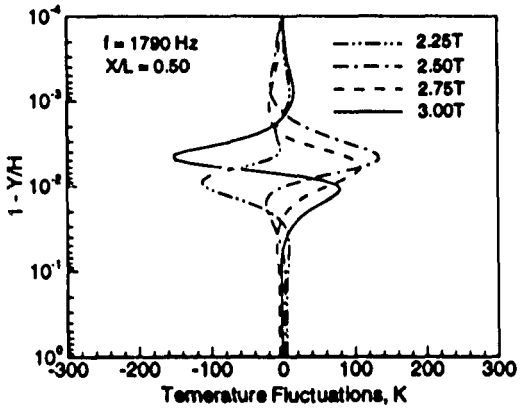

Figure 24: Time evolution of temperature fluctuations at axial location, X/L = 0.50

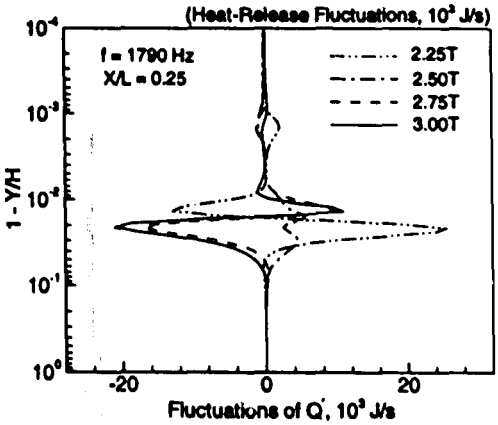

Figure 27: Time evolution of heat-release fluctuations at axial location, X/L = 0.25

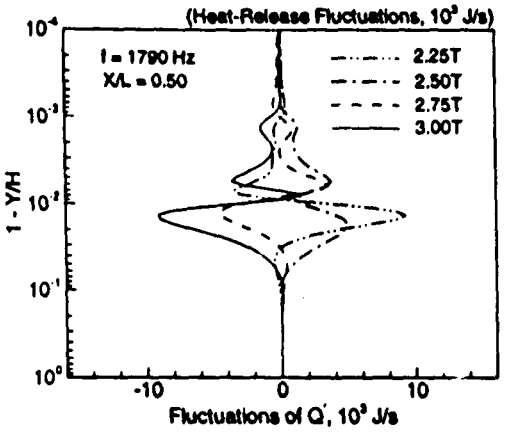

Figure 28: Time evolution of heat-release fluctuations at axial location, X/L = 0.50

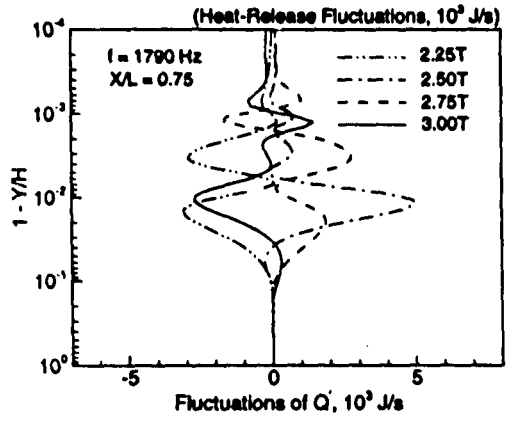

Figure 29: Time evolution of heat-release fluctuations at axial location, X/L = 0.75

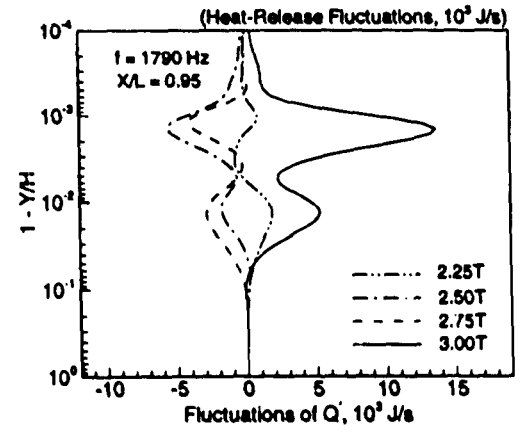

Figure 30: Time evolution of heat-release fluctuations at axial location, X/L = 0.95

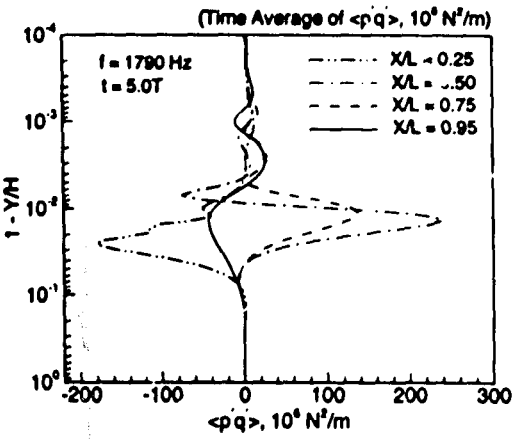

Figure 31: Time average of $< p'q' >$ at various axial locations

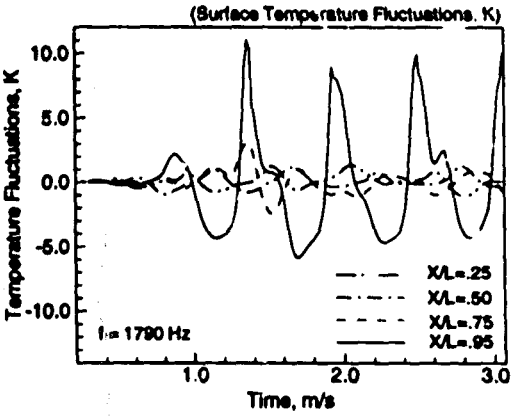

Figure 32: Time history of surface temperature fluctuations at various axial locations

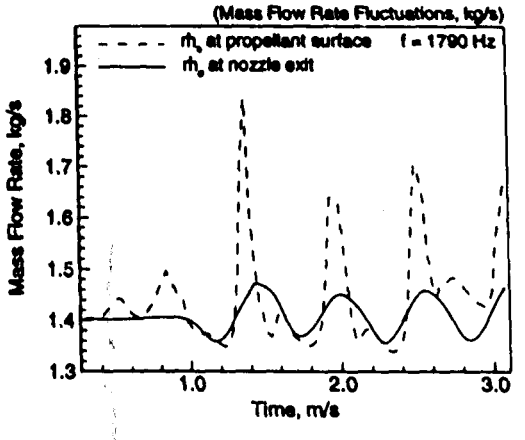

Figure 33: Time history of mass-flow rate fluctuations at propellant surface and nozzle exit